

## Effects of autoimmune abnormalities on skeletal muscle regeneration after needle puncture in mice

Misato Masugi<sup>1</sup>, Osamu Ichii<sup>1,2</sup> , Yuki Otani<sup>1</sup> , Takashi Namba<sup>1</sup>  and Yasuhiro Kon<sup>1</sup>

<sup>1</sup>Laboratory of Anatomy, Department of Basic Veterinary Sciences, Faculty of Veterinary Medicine, Hokkaido University, Sapporo 060-0818, Japan; <sup>2</sup>Laboratory of Agrobiomedical Science, Faculty of Agriculture, Hokkaido University, Sapporo 060-8589, Japan  
Corresponding author: Osamu Ichii. Email: ichi-o@vetmed.hokudai.ac.jp

### Impact statement

Mild traumatic injury of skeletal muscles is generally observed in the clinical field, such as intramuscular injection, and is characterized by muscle regeneration after immune cell infiltration. Therefore, autoimmune diseases could affect the repair process of traumatic skeletal muscle injury, but their pathological modification has been unclear. This study revealed the histopathological features of abdominal walls that received a needle puncture in an autoimmune disease mouse model. Infiltrations of lymphocytes, particularly T cells, around the injured muscle were substantially increased in mice with autoimmune disease. However, these muscles were regenerated without any abnormalities, such as fibrosis, with proliferation of fibro-adipogenic progenitors, in such mild injury. Therefore, this study provided the basic knowledge to understand the process and features of muscle regeneration in case of mild traumatic injuries in patients with autoimmune disease.

### Abstract

Regeneration of injured skeletal muscles is supported by the activation of satellite cells, and excessive traumatic injuries may trigger abnormal processes, such as fibrosis. Because the participation of immune cells is crucial during skeletal muscle repair, systemic autoimmune diseases impair their regeneration. This study focused on a traumatic injury by injection and investigated the effect of autoimmune diseases on skeletal muscle regeneration. Male mice of MRL/MpJ-*Fas*<sup>lpr/lpr</sup> and MRL/MpJ (6–7 months old) were used for autoimmune disease and healthy groups. The abdominal walls punctured by a needle were histologically analyzed at 1, 3, and 8 days postinjection. In both groups, injured skeletal muscle tissues showed necrosis and inflammatory cell infiltrations on day 1, increased cell density at 3 days, and regenerative myotubes with central nuclei without fibrosis at 8 days. Gr-1<sup>+</sup> neutrophils at injured skeletal muscle were abundant at 1 day, and then substantially decreased starting from 3 days in both groups. The number of CD3<sup>+</sup> T cells was remarkably higher in MRL/MpJ-*Fas*<sup>lpr/lpr</sup> than that in MRL/MpJ at 1 day, and a similar tendency was observed in B220<sup>+</sup> B cells. The numbers of IBA1<sup>+</sup> macrophages and bromodeoxyuridine-incorporating cells tended to be higher at 3 days, and those of the latter, mainly proliferating paired-box-7<sup>+</sup> satellite cells, showed significance at other time points and negatively correlated with the autoimmune disease indices, such as spleen weights or serum autoantibody level. Thus, this result suggested that injured skeletal muscle by minor trauma is normally regenerated regardless of the effects of autoimmune diseases, although lymphocyte infiltrations during these processes were more severe in MRL/MpJ-*Fas*<sup>lpr/lpr</sup>.

**Keywords:** Autoimmune disease, MRL/MpJ-*Fas*<sup>lpr/lpr</sup>, skeletal muscle, injection, muscle regeneration, histopathology

**Experimental Biology and Medicine 2023; 248: 1829–1840. DOI: 10.1177/15353702231198073**

### Introduction

Skeletal muscles continue regeneration and reconstruction to maintain their morpho-function during the lifetime. In a healthy status, skeletal muscles contain a pool of satellite cells, which are undifferentiated and quiescent mononuclear cells surrounding mature skeletal muscle cells. Their activation and differentiation are crucial for skeletal muscle regeneration accompanied by infiltrations of immune cells and activation of fibro-adipogenic progenitors (FAPs). FAPs are present in the skeletal muscle stroma, regulate immune cell accumulation and function, and influence the homeostasis of the satellite cell pool and myogenesis.<sup>1</sup> FAPs are

not myogenic cells, but have the bipotential abilities to differentiate into fibroblasts or adipogenic cells, and their cell fate is strongly affected by the external environment in the tissues.<sup>2,3</sup>

In a familiar environment, several skeletal muscle injuries are caused by accidents or medical treatments, such as surgery or intramuscular injection (i.m.). Generally, at the acute phase of traumatic skeletal muscle injury, myocytes undergo necrosis, and immune cells accumulate in response to skeletal muscle injury during the repair process. Neutrophils start to accumulate starting from 24 h after injury, followed by macrophage infiltration and satellite cell proliferation. From the data of a mouse model for severe traumatic skeletal

muscle injury,<sup>4</sup> C57BL/6 mice (B6) showed a predominant accumulation of CD11b-positive (CD11b<sup>+</sup>) cells at 3 days after injury induced by cardiotoxin (CTX) injection into the anterior tibial and quadriceps muscles. In this model, CD3<sup>+</sup>T cells increased at the injury site, and their numbers were maintained until day 5 after injection. At that time point, macrophage infiltrations switched from an inflammatory M1 to an anti-inflammatory M2 phenotype, and satellite cell proliferation reached its peak. Then, immune cells decreased whereas satellite cells showed self-duplication or formed centronuclear myotubes. Thus, the injured skeletal muscles were repaired by collaboration with the immune system.

However, several factors, such as genetic abnormalities, systemic diseases, and aging, cause the abnormalities of remodeling or regeneration, such as fibrosis, ossification, or adipogenesis in the skeletal muscle. For example, Schwartz-Jampel syndrome and muscular dystrophy are associated with genetic traits and cause skeletal muscle degeneration and abnormal regeneration.<sup>5</sup> Moreover, in traumatic skeletal muscle injury, in addition to a persistent infiltration of inflammatory cells, FAPs may proliferate and induce fibrosis,<sup>6</sup> even though they would normally trigger apoptosis. Therefore, traumatic injuries by medical treatments also induce the abnormalities of remodeling or regeneration in skeletal muscles. In medical settings, advances in acute care and traumatic surgery have increased the opportunities for medically induced traumatic skeletal muscle injuries. For example, surgical trauma to the jaw, such as bone resection, intramuscular injection, dental treatment, or surgery, is the most common cause of heterotopic ossification of the masticatory muscles and may cause deformity of the jaw joint.<sup>7</sup> Autoimmune diseases (AIDs) are characterized by the production of autoantibodies or autoreactive cells in response to tissues. The number of patients with AIDs is increasing each year.<sup>8</sup> Because skeletal muscle regeneration is related to the immune system, their abnormalities might be closely associated. Idiopathic myositis is an AID that targets skeletal muscle and is characterized by weakness, inflammation, and fibrosis of skeletal muscles.<sup>9</sup> However, the pathological correlation between autoimmune abnormalities and traumatic skeletal muscle injury remains unclear.

The pathological crosstalk between the immune system and skeletal muscle was mainly examined using severe experimental models induced by i.m. of myopathic reagents, such as CTX;<sup>10</sup> however, few studies have examined this crosstalk in milder skeletal muscle injury. In this study, we focused on needle puncture as a traumatic skeletal muscle injury and investigated the relationship between skeletal muscle remodeling or regeneration and autoimmune abnormalities using a mouse model. The results obtained from the present study revealed the effects of mild traumatic skeletal muscle injury on mice with healthy or autoimmune abnormalities. Therefore, this study provides crucial insight into evaluation of the effects of universally practiced medical treatments, particularly skeletal muscle needle puncture.

## Materials and methods

### Animals

Male MRL/MpJ (MpJ), MRL/MpJ-*Fas<sup>lpr/lpr</sup>* (lpr), and B6 mice were purchased from Japan SLC, Inc. (Hamamatsu, Japan) and maintained under specific pathogen-free conditions. Animal experimentation was approved by the Institutional Animal Care and Use Committee of the Faculty of Veterinary Medicine, Hokkaido University (approval No. 21-0008). All experimental animals were handled by the Guide for the Care and Use of Laboratory Animals, Faculty of Veterinary Medicine, Hokkaido University (approved by the Association for Assessment and Accreditation of Laboratory Animal Care International).

### Preparation of the abdominal wall puncture model

At 6–7 months of age, mice were weighed and anesthetized by intraperitoneal injection (i.p.) of a mixture of medetomidine (0.3 mg/kg), midazolam (4 mg/kg), and butorphanol (5 mg/kg) from the left area of the abdominal wall. Then, the abdominal skin was shaved and disinfected, and mice were gently kept warm and recovered by administering atipamezole (0.3 mg/kg, i.p.) with a 21G needle from the right-side abdominal wall. Then this area was recorded as a needle puncture site. Mice were euthanized 1, 3, or 8 days after the needle puncture, and tissue samples were collected (Figure 1(a)). All mice were administered bromodeoxyuridine (BrdU) (1 mg/10 g body weight (BW), i.p.) 2–3 h before they euthanized. Euthanasia was performed by cutting the femoral artery and dislocating the cervical vertebrae under deep anesthesia. The abdominal wall, including the external and internal oblique abdominal muscle and the transverse abdominis muscle, was collected without distinction because they were difficult to separately isolate. The right part of abdominal wall was used as the needle puncture site. Subsequently, the spleens were immediately collected and weighed.

### Serological analysis

For an index of AID development, serum levels of anti-double-stranded DNA (dsDNA) antibodies were measured to evaluate systemic autoimmune conditions using LBIS anti dsDNA-mouse ELISA kit (FUJIFILM Wako Pure Chemical Corporation; Osaka, Japan) according to manufacturer's instructions. As another index, the ratio of the spleen weight (SPW) to BW (SPW/BW) was calculated.

### Histological analysis

Needle puncture was performed perpendicular to the abdominal wall muscle, and the entire abdominal wall, including the punctured area, was subsequently collected. The abdominal wall was then stretched onto a flat surface, fixed in 4% paraformaldehyde overnight at 4°C, and embedded in paraffin. Longitudinal sections (3–4 μm thick) were cut through the abdominal wall muscle; each section therefore contained a transverse cross-section of the punctured

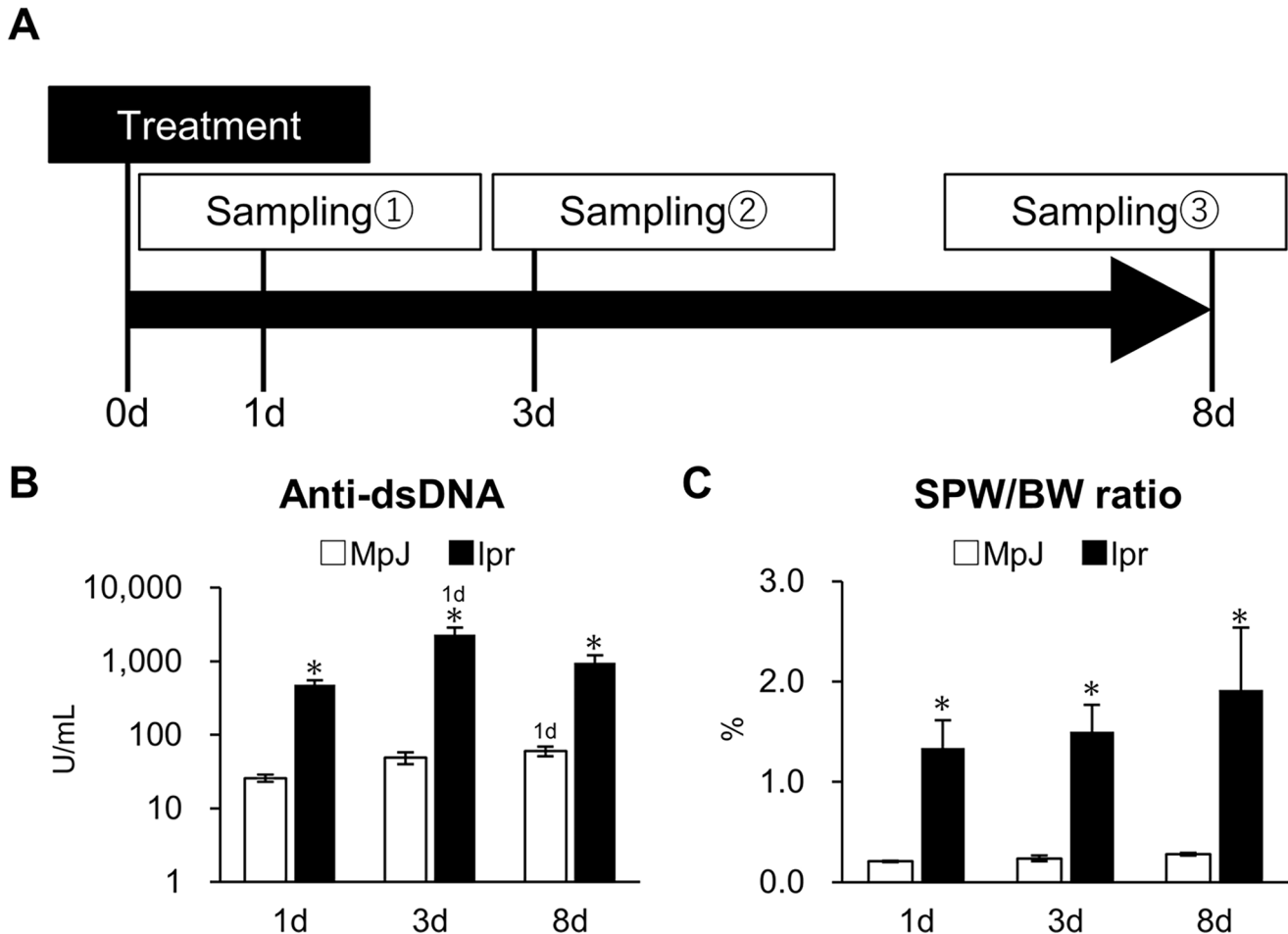


**Figure 1.** Experimental schedule and indices for autoimmune abnormalities. (a) Experimental schedule. (b) The serum levels of anti-double-stranded DNA (dsDNA) antibody. (c) The percentage of spleen weight (SPW) to body weight (BW). The number of samples used is as follows:  $n=5$  (MpJ/1 day), 4 (MpJ/3 days), 5 (MpJ/8 days), 4 (lpr/1 day), 4 (lpr/3 days), 4 (lpr/8 days). Each bar represents the mean  $\pm$  SE. \*: significant difference from the other strain at the same days that elapsed since puncture (Mann–Whitney  $U$ -test,  $*P < 0.05$ ). #: significant difference from the same strain at other days elapsed since puncture (Kruskal–Wallis test followed by Scheffé’s method,  $*P < 0.05$ ). MpJ: MRL/MpJ, lpr: MRL/MpJ-*Fas*<sup>lpr/lpr</sup>.

area. Deparaffinized sections were stained with hematoxylin–eosin (HE) or Elastica van Gieson (EVG), and the punctured area was identified by observing injured muscles.

#### Immunohistochemistry (IHC) and immunofluorescence (IF)

IHC for IBA1, Gr-1, B220, CD3, and BrdU was performed to detect the macrophages, neutrophils, B cells, T cells, and proliferating cells, respectively. Briefly, paraffin sections were deparaffinized, and antigen was retrieved by heating. Then, to block internal peroxidase activity, the sections were soaked in methanol containing 0.3%  $H_2O_2$  for 20 min at 25°C. After washing three times in phosphate-buffered saline (PBS), the sections were incubated with a blocking serum for 1 h at room temperature to block non-specific reactions. Then, sections were incubated with primary antibodies overnight at 4°C. After washing three times in PBS, the sections were incubated with secondary antibodies for 30 min at 25°C and washed three times in PBS. Consequently, the sections were incubated with streptavidin-conjugated horseradish peroxidase (SABPO® kit, Nichirei; Tokyo, Japan) for 30 min at 25°C, washed three times in PBS, and the immunopositive

reaction was visualized with 10 mg of 3,3'-diaminobenzidine tetrahydrochloride in 50 mL 0.05 M Tris- $H_2O_2$  solution. Finally, the sections were counterstained with hematoxylin. The details of the antibodies, antigen retrieval, and blocking are listed in Table 1.

IF was performed to detect BrdU-incorporating cells and positive cells for paired box 7 (PAX7) or platelet-derived growth factor receptor  $\alpha$  (PDGFR $\alpha$ ). The paraffin sections were deparaffinized, subjected to antigen retrieval, and then blocked using normal donkey serum, using the same protocol as that for IHC. After overnight incubation with the primary antibodies, sections were incubated with the secondary antibody for 1 h at 25°C. The sections were sealed with a water-soluble encapsulant and observed under fluorescence microscopy (BZX-710; Keyence; Osaka, Japan). The details of antigen retrieval, dilution, and source of antibodies are listed in Table 1.

#### Histoplanimetry

IHC sections were converted to virtual slides by Nano Zoomer 2.0 RS (Hamamatsu Photonics Co., Ltd.; Hamamatsu, Japan). Using NDP view2 (Hamamatsu Photonics Co., Ltd.), 3–5

**Table 1.** List of primary and secondary antibodies.

Antibody	Host	Dilution	Source	Retrieval	Blocking
IBA1	Rabbit	1:1200	Wako, Tokyo, Japan	CB	10% Goat normal serum
Gr-1	Rat	1:800	R and D system, Minnesota, USA	Pepsin	10% Goat normal serum
B220	Rat	1:1600	Cedarlane, Burlington, Canada	Tris	10% Goat normal serum
CD3	Rabbit	1:2*	Nichirei, Tokyo, Japan	Tris	10% Goat normal serum
BrdU	Rat	1:400	Abcam, Cambridge, UK	CB	5% Donkey normal serum (IHC) 10% Goat normal serum (IF)
Pax7	Mouse	1:1500	R and D system, Minnesota, USA	Tris	5% Donkey normal serum
PDGFR $\alpha$	Goat	1:300	R and D system, Minnesota, USA	Tris	5% Donkey normal serum
Rabbit IgG-biotin	Goat	Undiluted	SABPO(R) Kit, Nichirei, Tokyo, Japan		
Rat IgG-biotin	Goat	1:400	BioLegend, San Diego, CA, USA		
Rat IgG-Alexa Fluor 594	Donkey	1:500	Thermo Fisher Scientific, Waltham, MA, USA		
Mouse IgG- Alexa Fluor 546	Donkey	1:500	Thermo Fisher Scientific, Waltham, MA, USA		
Goat IgG- Alexa Fluor 488	Donkey	1:500	Thermo Fisher Scientific, Waltham, MA, USA		

CB: 10 mM citrate buffer (pH=6.0), 110°C, 15 min. Tris: 20 mM Tris-HCl (pH=9.0), 110°C, 15 min. Pepsin: 0.1% pepsin/0.2 M HCl, 37°C, 5 min; IHC: immunohistochemistry; IF: immunofluorescence.

\*Prediluted antibody.

images of the puncture site were randomly selected at 40 $\times$  magnification. Then, the number of total and positive cell nuclei in necrotic areas was manually identified in the IHC-stained images of IBA1, Gr-1, B220, CD3, and BrdU. Each percentage of the number of positive cell nuclei to total cell nuclei in the injury region was calculated. Because of the strong nonspecific response of IBA1 to necrotic cytoplasm, BZ-X710 and BZ-H3C (Keyence) color discrimination was used to identify positive cells.

### Statistical analysis

The results were expressed as the mean  $\pm$  standard error (SE) and analyzed by non-parametric statistical methods. Significant difference between two groups was assessed by Mann-Whitney *U* test. Kruskal-Wallis test was used to compare the numerical results, and multiple comparisons were performed using Dunnett's test when significant differences were observed. The correlation was analyzed using Spearman's correlation test. A *P*-value lower than 0.05 was regarded as a significant difference in all analyses. All statistical analysis was performed using IBM SPSS ver. 28.0.1 (IBM Japan Ltd., Tokyo, Japan).

## Results

### Indices of AID

According to Figure 1(a), treatment and sampling were performed at 1, 3, and 8 days. Serum levels of anti-dsDNA antibody and the ratio of SPW/BW of 6–7 month-old MpJ and lpr mice were measured at each time point as indices of AID (Figure 1(b) and (c)). Lpr mice showed significantly higher values compared with those of MpJ mice in both indices at all time points (note logarithmic display). Furthermore, MpJ mice at 8 days and lpr mice at 3 days showed significantly higher serum levels of anti-dsDNA antibody compared to each value at 1 day. These data indicated that the lpr mice used in this experiment developed a systemic AID.

### Histological alterations of the puncture region over time

As shown in the images of HE-stained section from MpJ at 1 day (Figure 2(a)), the injured myofibers at the puncture region showed necrosis and a paler color compared with that of the surrounding intact myofibers. These alternations were observed along with the longitudinal axis of injured myofibers and separated the injured and healthy skeletal muscle tissue. Therefore, these necrotic areas were defined as the injured area surrounded by healthy myofibers.

Figure 2(b) shows the HE-stained cross sections of the abdominal wall muscle, including the injured area, and summarizes the histological alternations of MpJ and lpr mice during the observation period. Briefly, MpJ and lpr mice showed similar histological alterations. On day 1, the injured myofibers were necrotic with a few scattered infiltrations of inflammatory cells and blood cells. On day 3, abundant mononuclear cell infiltrations were observed between the necrotic myofibers, indicating induction of local inflammatory response. On day 8, the number of infiltrating cells decreased, and many regenerative myotubes with central nuclei were observed. Thus, comparable histological changes in the injury and regenerative process of skeletal muscles by needle puncture were observed, and the features of inflammatory response at 3 days and regeneration at 8 days were prominent in both strains.

### Inflammatory cell infiltration at the puncture region

Next, we assessed macrophages and neutrophils, which are known to be initially induced in the region of skeletal muscle injury.<sup>11</sup> Moreover, B and T cells were examined to evaluate their relationship with AIDs.

As shown in Figure 3, IBA1<sup>+</sup> macrophages were abundantly observed at 3 days among all examined inflammatory cells in both strains and tended to be comparable or decreased at 8 days (Figure 3(a)). However, common to both strains, abundant Gr-1<sup>+</sup> neutrophils were observed at 1 day and decreased onward (Figure 3(b)). Quantification of



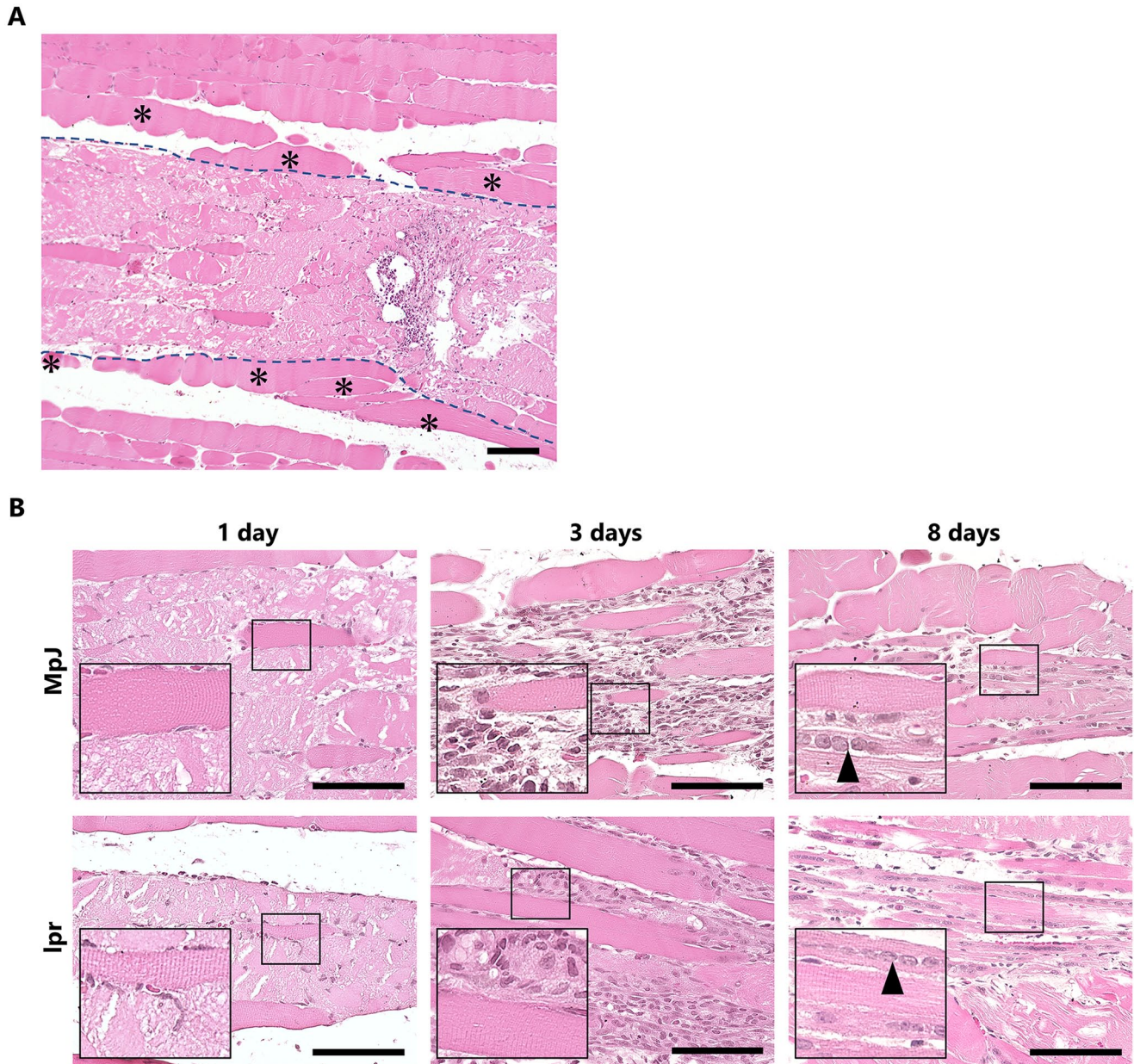


**Figure 2.** Histological features of myofibers in the injury region after needle puncture in the muscle. (a) Histological features of the abdominal wall muscle of MpJ mice at 1 day around the puncture region. The blue line represents the boundary between the injury and healthy regions. Myofibers at the injury region have necrotic cytoplasm. Bars = 100  $\mu$ m. \*: Normal myofibers. (b) Histological alternations at the injury region of MpJ and lpr mice over time. Both strains show cellular infiltration owing to inflammatory response at 3 days. At 8 days, the number of infiltrating cells decreases, and many regenerative myotubes with central nuclei are observed (arrowheads). Insets indicate the squared area. Bars = 100  $\mu$ m. Hematoxylin–eosin staining. MpJ: MRL/MpJ, lpr: MRL/MpJ-*Fas*<sup>lpr/lpr</sup>.

these inflammatory cells showed that IBA1<sup>+</sup> macrophages exhibited the highest values at 3 days in both strains without strain- or time course-related significant differences (Figure 3(c)). For Gr-1<sup>+</sup> neutrophils, the quantitative values at one day were significantly higher than those at other time points in both strains without strain differences (Figure 3(d)).

As shown in Figure 4(a) and (b), the number of lymphocytes was lower than that of macrophages and neutrophils, but some differences were detected between studied strains. Briefly, the quantification of these cells showed no change in B220<sup>+</sup> B cells of MpJ mice during the observation periods, but lpr mice showed the highest values at 1 day with a higher

tendency compared with that of MpJ ( $P=0.063$ ) and then decreased (Figure 4(c)). Similar tendency was also observed in CD3<sup>+</sup> T cells, and lpr mice showed a significantly higher value compared with that of MpJ at 1 day and then decreased (Figure 4(d)). Thus, lpr mice were suggested to induce more lymphocyte infiltration among injured myofibers at 1 day compared with that of MpJ mice.

#### Proliferating cells at the puncture region

During skeletal muscle regeneration, the formation of myotubes by proliferation, differentiation, and fusion of satellite cells is important.<sup>12</sup>



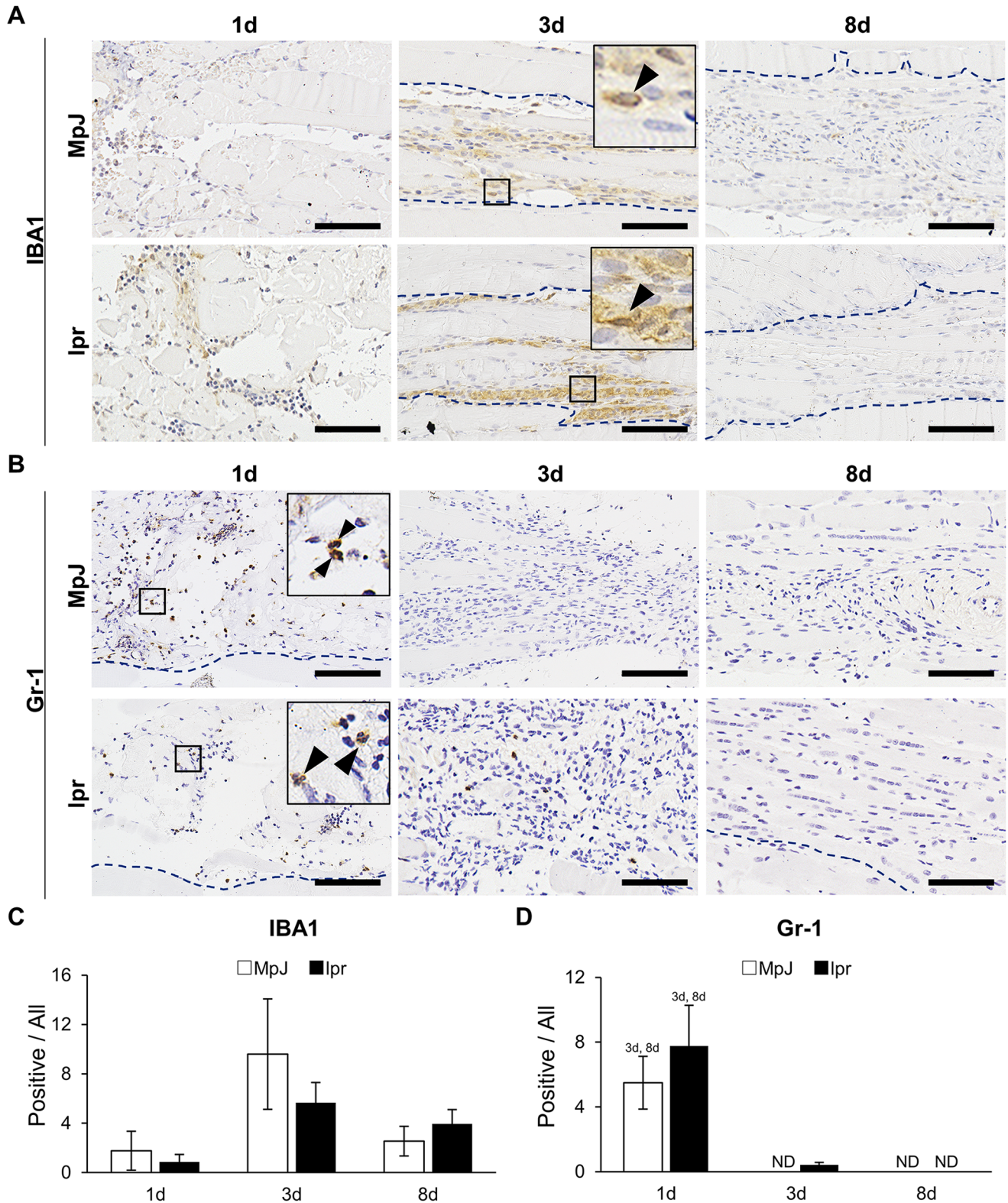


**Figure 3.** Infiltration of macrophages and neutrophils at the injury region after needle puncture in the muscle. (a) IBA1-positive macrophages (arrowheads). More cells are observed at 3 days in both strains. (b) Gr-1-positive neutrophils (arrowheads). More cells are observed at 1 day in both strains. Immunohistochemistry staining. Bars = 100  $\mu$ m. The blue line represents the boundary between the injury and healthy regions. (c) The percentage of the number of IBA1-positive cell nuclei to that of all cell nuclei in the injury region. (d) The percentage of the number of Gr-1-positive cell nuclei to that of all cell nuclei in the injury region. ND: Not detected. The number of samples used is as follows:  $n=5$  (MpJ/1 day), 5 (MpJ/3 days), 5 (MpJ/8 days), 4 (lpr/1 day), 5 (lpr/3 days), 4 (lpr/8 days). Each bar represents the mean  $\pm$  SE. 3d, 8d: significant difference from the same strain at 3 days and 8 days since puncture (Kruskal–Wallis test followed by Scheffé’s method,  $^{\#}P < 0.05$ ). MpJ: MRL/MpJ, lpr: MRL/MpJ-*Fas<sup>lpr/lpr</sup>*.



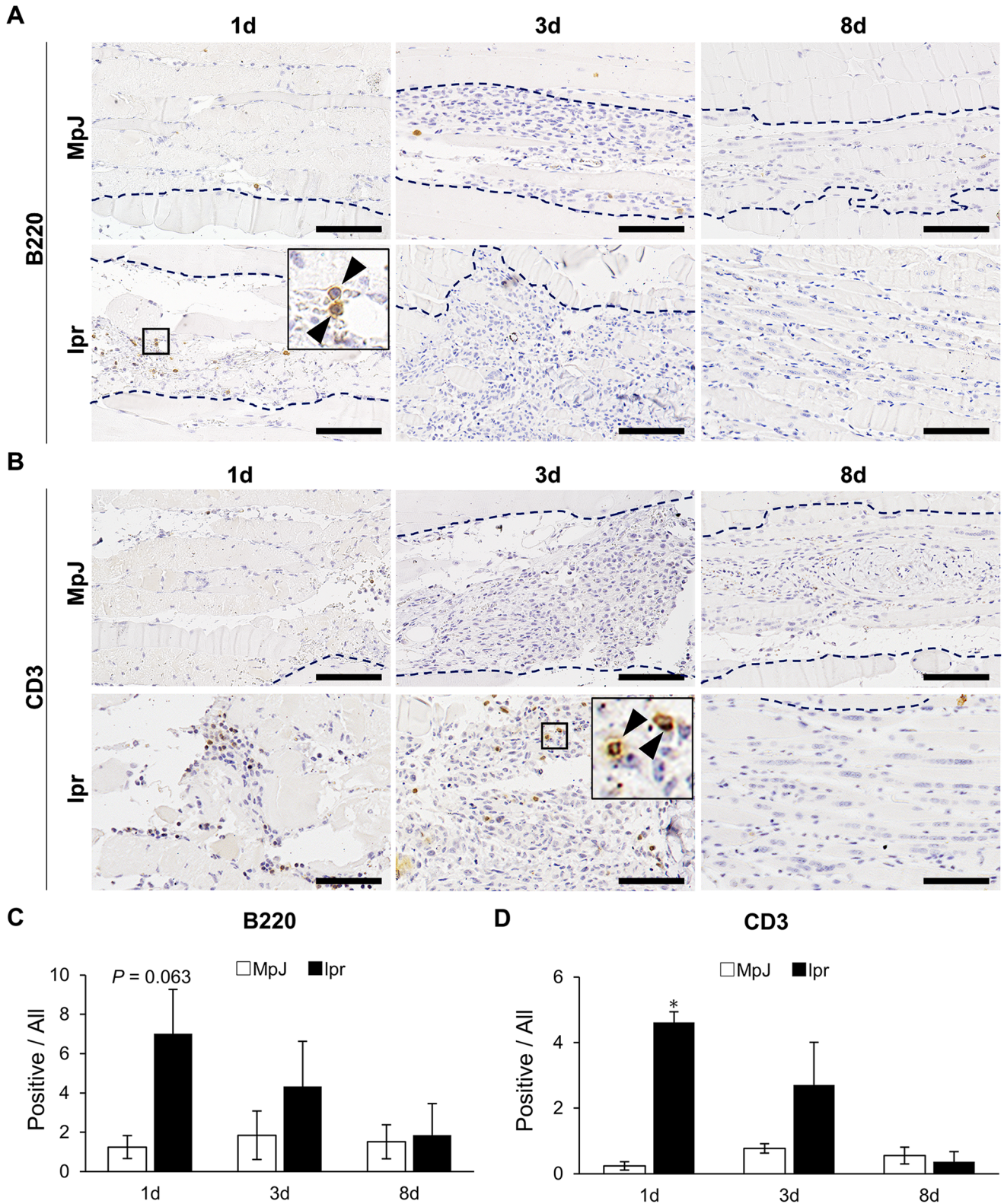


**Figure 4.** Infiltration of lymphocytes at the injury region after needle puncture in the muscle. (a) B220-positive B cells (arrowheads). Slightly more cells are observed in lpr at 1 day. (b) CD3-positive T cells (arrowheads). More cells are observed in lpr at 1 day. Immunohistochemistry staining. Bars = 100  $\mu$ m. The blue line represents the boundary between the injury and healthy regions. (c) The percentage of the number of B220-positive cell nuclei to that of all cell nuclei in the injury region. (d) The percentage of the number of CD3-positive cell nuclei to that of all cell nuclei in the injury region. The number of samples used is as follows:  $n = 5$  (MpJ/1 day), 5 (MpJ/3 days), 5 (MpJ/8 days), 4 (lpr/1 day), 5 (lpr/3 days), 4 (lpr/8 days). Each bar represents the mean  $\pm$  SE. \*: significant difference from the other strain at same days elapsed since puncture (Mann-Whitney  $U$ -test,  $*P < 0.05$ ). MpJ: MRL/MpJ, lpr: MRL/MpJ-Fas<sup>lpr/lpr</sup>.

Figure 5(a) shows the IHC images of BrdU-incorporating proliferating cells in the puncture region of MpJ and *lpr* mice. Few positive cells were detected at 1 day in both strains, but they were observed as numerous at 3 days and tended to decrease at 8 days. Quantification of BrdU-incorporating cells (Figure 5(b)) showed that the values in MpJ were significantly higher at 3 days compared with those at 1 and 8 days. *lpr* mice also showed a similar tendency, and a significant difference was observed between 1 and 3 days. Further, the values at 3 days tended to be higher in MpJ than those in *lpr* mice ( $P=0.095$ ).

Next, the cell type of BrdU-incorporating cells was investigated by assessment of IF. PAX7 and PDGFR $\alpha$ , which were used as markers for satellite cell activation from quiescent to proliferative stages and for FAPs, which are mesenchymal progenitor cells known to influence myogenesis by regulating immune cell accumulation and function and by providing extracellular matrix components.<sup>2,13</sup> In both strains, almost all PAX7<sup>+</sup> nuclei showed the merged reactions with BrdU-incorporating nuclei during the observation period (Figure 5(c)). However, PDGFR $\alpha$ <sup>+</sup> cells rarely showed BrdU incorporation (Figure 5(c)). This suggests that many satellite cells have been activated from the quiescent to the proliferative phase at the 3 days injury region.

To confirm the influence of the genetic background of the mice, the same experiment was conducted with B6 mice (Supplemental Figure 1). We found that all BrdU-incorporating nuclei observed were PAX7<sup>+</sup> nuclei at 3 days, similar to MpJ and *lpr* mice.

### Verification of fibrosis as a regenerative abnormality

Finally, to examine the fibrosis associated with the skeletal muscle injury, EVG-stained sections were observed. Figure 6 shows EVG-stained cross sections of the abdominal wall muscle, including the injured area, and summarizes the histological alterations over time in MpJ and *lpr* mice. At 1 day, it showed a decrease in the staining intensity of picric acid<sup>+</sup> myofibers at the injury region owing to necrosis, and a very small amount of collagen fibers were observed in the interstitium of the skeletal muscles. At 3 days, there was a notable increase in collagen fibers, and the necrotic tissue showed abundant cells, including infiltrating cells. However, at 8 days, when skeletal muscle regeneration was initiated, centronuclear myocytes (as shown in Figure 2(b)) were formed similarly to normal myofibers, and a significant decrease in collagen fibers was observed, confirming a smooth regeneration process. Thus, in both strains, no fibrotic features were detected in the injury region, indicating normal regeneration of skeletal muscles.

### Discussion

This study aimed to clarify the effects of systemic immunological abnormalities on the repair processes of injured skeletal muscles. In particular, the authors focused on traumatic skeletal muscle injuries that are universally caused by medical treatments, such as i.m. The skeletal muscles of

abdominal walls in AID-prone *lpr* mice were punctured. Their histological alterations with immunological indices at several time points were compared with those of MpJ, a healthy control strain of *lpr* mice. Although both strains showed similar skeletal muscle injuries and regeneration without fibrotic features, several features, such as lymphocyte infiltration dynamics, were different in these processes.

Several studies using mouse models with CTX- or glycerol-induced muscle injuries indicated that satellite cell activation continued up to day 4 after injury, myotubes with central nuclei were evident at day 7, and the diameter of these myotubes continued to increase until day 14.<sup>14</sup> In particular, the CTX model is suitable for studying uniform and complete regeneration. Fibrosis is mild and transient, and the CTX model is used globally. However, experimental glycerol myopathy could be a suitable model to study the pathophysiology of Duchenne muscular dystrophy, where impaired regeneration is observed, and fibrosis occurs. In the present study, we focused on needle puncture as a traumatic skeletal muscle injury and investigated the relationship between the remodeling or regeneration of skeletal muscle and autoimmune abnormalities using a mouse model; therefore, we compared the result from CTX-model with our obtained data.

In this study, sampling points were scheduled at day 1 (immediately after injury/acute inflammation), day 3 (active inflammation), and day 8 (regeneration) to elucidate the effects of AID on muscle injury inflammation and regeneration, with a particular focus on the cells localized to puncture lesions. Although fibrosis starts at day 4 due to the proliferation of fibroblasts in more severe cases,<sup>14</sup> no significant collagen deposition was noted in our model on days 3 and 8 after puncture. Furthermore, on day 8, there was no significant difference in the regeneration features (see Figures 2, 5, and 6). Therefore, we concluded that fibrosis, as indicated by the proliferations of PDGFR $\alpha$ <sup>+</sup> cells, did not occur in both healthy and AID groups in this puncture model.

For examined indices of autoimmune abnormalities, the serum level of anti-dsDNA antibody was gradually and significantly increased in MpJ mice from 1 to 8 days, and this increase was more prominent in *lpr* mice from 1 to 3 days. For supportive data, correlation analysis was performed between indices of AID and the quantitative values of examined cells (Supplemental Table 1). Although no significant correlation was observed within each group, the numbers of CD3<sup>+</sup> T cells and B220<sup>+</sup> B cells temporarily increased at 1 and 3 days, respectively, when the serum level of the anti-dsDNA antibody increased. This result was observed using all groups. Myositis autoantigens, such as histidyl tRNA synthetase, Mi-2, U1-70kD, Ku/the catalytic subunit of DNA-dependent protein kinase, are expressed at high levels in myositis skeletal muscles, whereas they are very low in normal skeletal muscles; their expressions are increased in cells that have features of regenerating skeletal muscle cells.<sup>15</sup> Furthermore, traumatic skeletal muscle injury stimulates the production of autoantibodies following inflammation.<sup>16</sup> Therefore, the authors supposed that *lpr* mice also developed myositis with the increase of serum autoantibodies, such as an anti-dsDNA antibody, by the increase of this autoantigen expression after



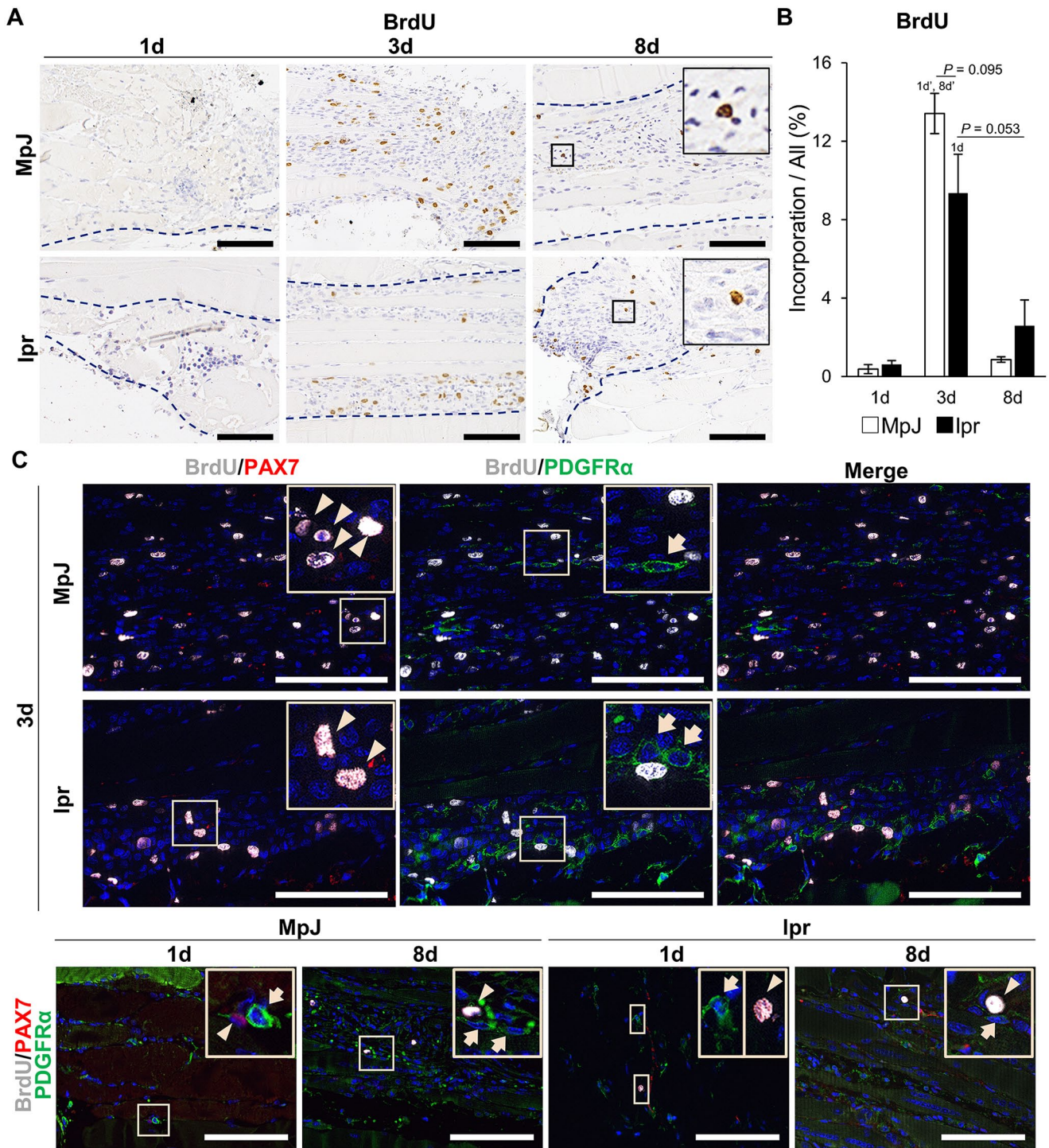


**Figure 5.** Proliferating cells in the injury region after needle puncture in the muscle. (a) Bromodeoxyuridine (BrdU)-incorporating cells (arrowhead). The blue line represents the boundary between the injury and healthy regions. More cells are observed at 3 days in both strains. Immunohistochemistry staining. Bars = 100  $\mu$ m. (b) The percentage of the number of BrdU-incorporating cell nuclei to that of all cell nuclei in the injury region. The number of samples used is as follows:  $n=5$  (MpJ/1 day), 5 (MpJ/3 days), 5 (MpJ/8 days), 4 (lpr/1 day), 5 (lpr/3 days), 4 (lpr/8 days). Each bar represents the mean  $\pm$  SE. 1d, 1d', 8d': significant difference from the same strain at other days elapsed since puncture (Kruskal–Wallis test followed by Scheffé's method, 1d  $P < 0.05$ , 1d' 8d'  $P < 0.01$ ). Significant differences from the other strain at same days are analyzed by Mann–Whitney  $U$ -test. (c) Double immunofluorescence (IF) for BrdU (white/ proliferating cells) and paired box 7 (PAX7) (red/satellite cells) or platelet-derived growth factor receptor  $\alpha$  (PDGFR $\alpha$ ) (green/ fibro-adipogenic progenitors) at 3 days, 1 and 8 days. At 3 days, almost all BrdU-incorporating cells are merged with PAX7-positive cells (arrowhead), not PDGFR $\alpha$ -positive cells (arrow) in both strains. Similarly, at 1 and 8 days, both PAX7-positive cells and PDGFR $\alpha$ -positive cells are localized at the injury region, and BrdU-incorporating cells merged with only PAX7 in both strains. Blue: Hoechst (nuclei). Bars = 100  $\mu$ m. MpJ: MRL/MpJ, lpr: MRL/MpJ-*Fas*<sup>lpr/lpr</sup>.

skeletal muscle injuries. However, the myositis feature was not clearly observed in lpr mice, and the skeletal muscle inflammation was mild and limited in a locally injured area

and eventually diminished at 8 days. Therefore, AID-prone mice induced the production of anti-dsDNA antibodies more abundantly compared with that in healthy ones after skeletal



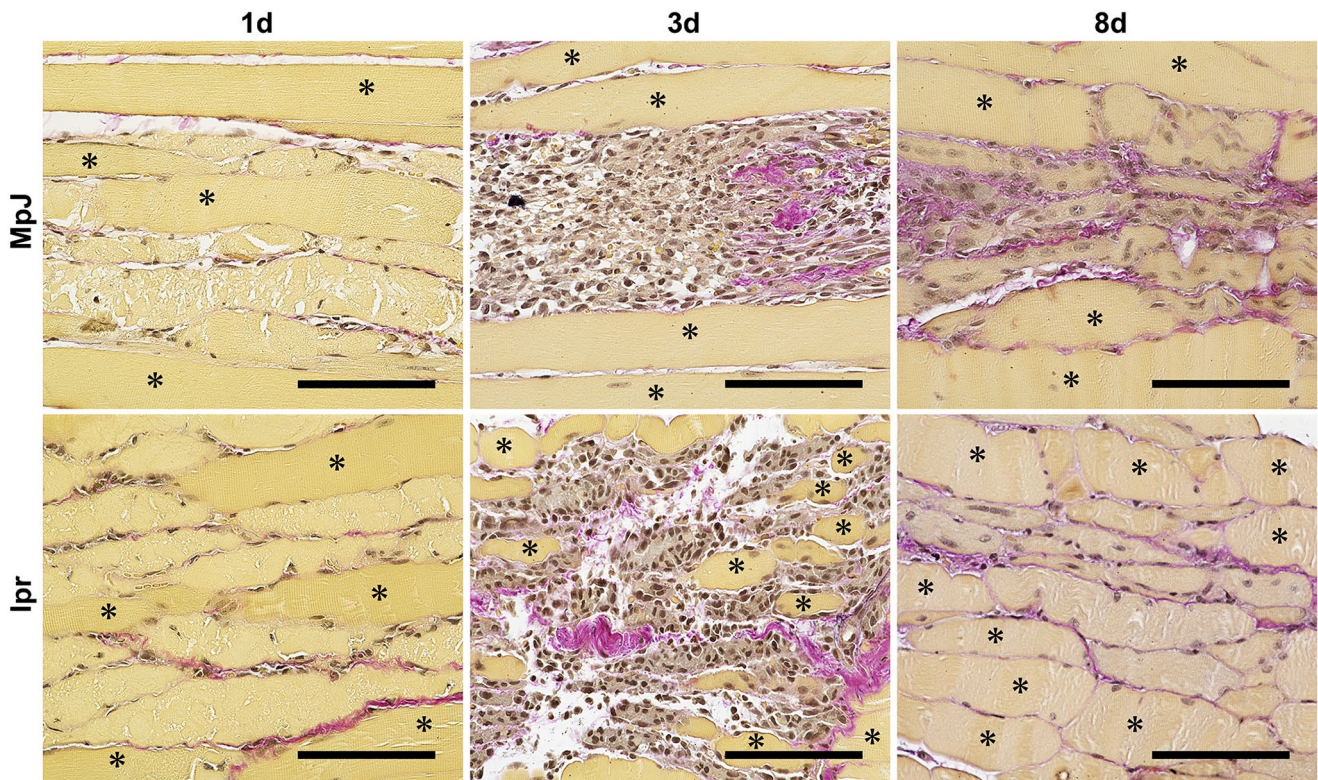


**Figure 6.** Histological evaluation of fibrosis in the injury region after needle puncture in the muscle. Fibrosis of the abdominal wall muscle is examined at the injury region of MpJ and lpr mice over time. No fibrotic features are detected in the injury region in both strains. Collagen fibers are stained as purple. Elastica van Gieson staining. \*(yellow): Normal myofibers. Bars= 100  $\mu$ m. MpJ: MRL/MpJ, lpr: MRL/MpJ-*Fas<sup>pr/lpr</sup>*.

muscle injuries although they did not develop myositis. Furthermore, the authors assumed that the pathological effects on systemic organs by autoantibody increase might be mild after local traumatic skeletal muscle injury because no significant alteration was detected in the ratio of SPW/BW from 1 to 3 days in both strains.

Traumatic skeletal muscle injuries in both strains resulted in infiltration of immune cells that contribute to innate immune responses, such as neutrophils and macrophages. However, it was characterized by a more abundant infiltration of lymphocytes, especially T cells, in lpr mice. T cells (CD45<sup>+</sup> CD11b<sup>-</sup> CD3<sup>+</sup> cells) infiltrate the skeletal muscle after injury, and their number in the skeletal muscle peaked at 3 days and remained constant through 5 days before declining at 7 days by one CTX injection to the anterior tibialis and quadriceps muscles of 8- to 10-week-old female B6 mice. Furthermore, it was suggested that they activated T helper cells, consistently expressing CD4 but not CD8 marker.<sup>4</sup> Importantly, lpr mice developed progressive lymphadenopathy after 6 weeks of age owing to accumulation of an abnormal population of CD4<sup>-</sup> CD8<sup>-</sup> double-negative T cells.<sup>17,18</sup> It is unclear whether these lymphocytes in lpr mice recognized specific antigens derived from the destroyed myocytes or this was the result of a nonspecific immune response; however, the lpr mutation itself and/or the associated autoimmune abnormalities would affect the infiltration of lymphocytes, especially T cells, at the injured skeletal muscle area.

Many myogenic progenitor cells and FAPs were detected as BrdU-incorporating cells at 3–4 days during

the regeneration process after extensive skeletal muscle disruption with CTX i.m. to the hindlimbs of B6 mice.<sup>3</sup> FAPs are quiescent in intact skeletal muscle but proliferate in response to skeletal muscle injury to stimulate activation and differentiation of satellite cells.<sup>3,19,20</sup> Therefore, in this study, PAX7<sup>+</sup> satellite cells and PDGFR $\alpha$ <sup>+</sup> FAPs were co-stained, but only the formers proliferated at the injury site after puncture in both groups. Considering the influence of the genetic background of the mice on this phenotype, the same experiments were conducted with B6 mice (Supplemental Figure 1); the results showed that, similar to MpJ and lpr mice, all BrdU-incorporating cells were satellite cells, and FAPs did not show incorporation. Therefore, it was concluded that FAPs activation is not induced in skeletal muscle injury by puncture, although satellite cells locally proliferate. Regarding the differences from previous studies using the CTX i.m. model,<sup>3,19,20</sup> the variation in the degree of skeletal muscle injury, rather than the genetic background of the mice, was considered to affect the proliferation kinetics of satellite cells and FAPs.

In healthy skeletal muscle tissue, satellite cells go from a quiescent state to a proliferative phase a few days after injury and simultaneously start to repair the injured and necrotic sites.<sup>3,21</sup> Increased proliferating cells at the injury site at 3 days tended to be less in lpr than those in MpJ mice. Importantly, the autoantibody concentration of healthy MpJ mice progressively increased up to 8 days. Because the majorities of the proliferating cells are satellite cells, the change in MpJ autoantibody concentration may have reflected a transient

increase in regenerating myocytes expressing autoreactive autoantigen.<sup>14,22</sup> However, at 3 days, lpr tended to have the same or fewer proliferating cells as those in MpJ mice, and correlation analysis of all mice showed a negative correlation between the index of AID and the number of proliferating cells. However, the increased autoantibody concentration at 3 days was more remarkable in lpr than that in MpJ mice, suggesting that this phenotype reflects excessive activation of the immune system to recognize the autoantigen rather than the amount of autoantigen derived from the regenerating myocytes.<sup>23</sup> In addition, satellite cells and FAPs in healthy skeletal muscle tissue distant from the injury site were compared between MpJ and lpr mice, but no difference was detected in their number or localization (data not shown).

Both strains had no remarkable fibrosis findings at the injury site. Essentially, fibrosis occurs in damaged skeletal muscle when persistent inflammatory cell infiltration and fibroblast activation produce a mass of nonfunctional fibrous tissue.<sup>24,25</sup> Apoptosis of FAPs is required for normal skeletal muscle regeneration and the failure of apoptosis leads to skeletal muscle fibrosis by increasing the survival rate of FAPs.<sup>19,20</sup> However, in this study, neither proliferation of FAPs nor fibrosis were detected. Thus, it can be assumed that AIDs affect lymphocyte induction and satellite cell dynamics in the early stages of injury, whereas minor skeletal muscle injuries, such as puncture, do not directly lead to fibrosis or other regenerative abnormalities.

In conclusion, this study demonstrated that autoimmune abnormalities modified the processes of inflammation and repair after skeletal muscle injury, whereas the skeletal muscles injured by mild trauma, such as needle puncture can be normally regenerated. This might suggest that the induction of immune-associated abnormal skeletal muscle regeneration is affected by the kinds of reagents or adjuvants rather than the puncture itself, whereas the accumulation of data from various conditions and diseases would be crucial. The obtained results also emphasized an important perspective for future studies, especially focusing on the significance of less invasive medical treatment for patients with autoimmune abnormalities.

This study did not address the long-term effect of muscle puncture on AID status. Furthermore, a future study into how muscle-derived autoantigens influence systemic AID phenotypes would help comprehensively elucidate the effect of muscle puncture on AID and vice versa (e.g. muscle puncture before AID development at a young age, and analysis at 6–8 months of age using MRL/lpr) with functional effects, such as muscle contractility.

#### AUTHORS' CONTRIBUTIONS

MM, OI, and YK designed and performed the experiments. MM, YO, and TN provided the samples and analyzed the data. All authors were involved in writing the paper and have approved the final manuscript.

#### DECLARATION OF CONFLICTING INTERESTS

The author(s) declared no potential conflicts of interest with respect to the research, authorship, and/or publication of this article.

#### FUNDING

The author(s) received no financial support for the research, authorship, and/or publication of this article.

#### ORCID IDS

Osamu Ichii  <https://orcid.org/0000-0002-6643-1554>

Yuki Otani  <https://orcid.org/0000-0003-0224-6197>

Takashi Namba  <https://orcid.org/0000-0001-5368-2672>

#### SUPPLEMENTAL MATERIAL

Supplemental material for this article is available online.

#### REFERENCES

- Heredia JE, Mukundan L, Chen FM, Mueller AA, Deo RC, Locksley RM, Rando TA, Chawla A. Type 2 innate signals stimulate fibro/adipogenic progenitors to facilitate muscle regeneration. *Cell* 2013;**153**:376–88
- Uezumi A, Fukada SI, Yamamoto N, Takeda S, Tsuchida K. Mesenchymal progenitors distinct from satellite cells contribute to ectopic fat cell formation in skeletal muscle. *Nat Cell Biol* 2010;**12**:143–52
- Joe AWB, Yi L, Natarajan A, le Grand F, So L, Wang J, Rudnicki MA, Rossi FMV. Muscle injury activates resident fibro/adipogenic progenitors that facilitate myogenesis. *Nat Cell Biol* 2010;**12**:153–63
- Castiglioni A, Corna G, Rigamonti E, Basso V, Vezzoli M, Monno A, Almada AE, Mondino A, Wagers AJ, Manfredi AA, Rovere-Querini P. FOXP3+ T cells recruited to sites of sterile skeletal muscle injury regulate the fate of satellite cells and guide effective tissue regeneration. *PLoS One* 2015;**10**:e0128094
- Chandra SR, Issac TG, Gayathri N, Shivaram S. Schwartz–Jampel syndrome. *J Pediatr Neurosci* 2015;**10**:169–71
- Ieronimakis N, Hays A, Prasad A, Janebodin K, Duffield JS, Reyes M. PDGFR $\alpha$  signalling promotes fibrogenic responses in collagen-producing cells in Duchenne muscular dystrophy. *J Pathol* 2016;**240**:410–24
- Schoenmaker T, Dahou Bouchankouk A, Özkan S, Gilijamse M, Bouvy-Berends E, Netelenbos C, Lobbezoo F, Eekhoff EMW, de Vries TJ. Limitations of jaw movement in fibrodysplasia ossificans progressiva: a review. *Front Med* 2022;**9**:852678
- Bach JF. The effect of infections on susceptibility to autoimmune and allergic diseases. *N Engl J Med* 2002;**347**:911–20
- Torres-Ruiz J, Alcalá-Carmona B, Alejandre-Aguilar R, Gómez-Martín D. Inflammatory myopathies and beyond: the dual role of neutrophils in muscle damage and regeneration. *Front Immunol* 2023;**14**:1113214
- Hardy D, Besnard A, Latil M, Jouvion G, Briand D, Thépenier C, Pascal Q, Guguin A, Gayraud-Morel B, Cavaillon JM, Tajbakhsh S, Rocheteau P, Chrétien F. Comparative study of injury models for studying muscle regeneration in mice. *PLoS One* 2016;**11**:e0147198
- Tidball JG, Villalta SA. Regulatory interactions between muscle and the immune system during muscle regeneration. *Am J Physiol Regul Integr Comp Physiol* 2010;**298**:R1173–87
- Hawke TJ, Garry DJ. Myogenic satellite cells: physiology to molecular biology. *J Appl Physiol* 2001;**91**:534–51
- Seale P, Sabourin LA, Girgis-Gabardo A, Mansouri A, Gruss P, Rudnicki MA. Pax7 is required for the specification of myogenic satellite cells. *Cell* 2000;**102**:777–86
- Mohamed AAA. Glycerol-induced injury as a new model of muscle regeneration. *Cell Tissue Res* 2018;**374**:233–41
- Casciola-Rosen L, Nagaraju K, Plotz P, Wang K, Levine S, Gabrielson E, Corse A, Rosen A. Enhanced autoantigen expression in regenerating muscle cells in idiopathic inflammatory myopathy. *J Exp Med* 2005;**201**:591–601
- Sciorati C, Rigamonti E, Manfredi AA, Rovere-Querini P. Cell death, clearance and immunity in the skeletal muscle. *Cell Death Differ* 2016;**23**:927–37
- Matsumoto K, Sakamoto Y, Hirose S. Granulocytosis and its correlation to lymphoproliferative disorder in autoimmune-prone MRL/lpr mice. *Juntendo Med J* 1989;**35**:106–16



18. Singer GG, Carrera AC, Marshak-Rothstein A, Martínez-AC, Abbas AK. Apoptosis, fas and systemic autoimmunity: the MRL-Ipr/Ipr model. *Curr Opin Immunol* 1994;**6**:913–20
19. Lemos DR, Babaeijandaghi F, Low M, Chang CK, Lee ST, Fiore D, Zhang RH, Natarajan A, Nedospasov SA, Rossi FMV. Nilotinib reduces muscle fibrosis in chronic muscle injury by promoting TNF-mediated apoptosis of fibro/adipogenic progenitors. *Nat Med* 2015;**21**:786–94
20. Chikenji TS, Saito Y, Konari N, Nakano M, Mizue Y, Otani M, Fujimiya M. p16<sup>INK4A</sup>-expressing mesenchymal stromal cells restore the senescence-clearance-regeneration sequence that is impaired in chronic muscle inflammation. *EBioMedicine* 2019;**44**:86–97
21. Garry DJ, Meeson A, Elterman J, Zhao Y, Yang P, Bassel-Duby R, Williams RS. Myogenic stem cell function is impaired in mice lacking the forkhead/winged helix protein MNF. *Proc Natl Acad Sci U S A* 2000;**97**:5416–21
22. Mohassel P, Rosen P, Casciola-Rosen L, Pak K, Mammen AL. Expression of the dermatomyositis autoantigen transcription intermediary factor 1 $\gamma$  in regenerating muscle. *Arthritis Rheumatol* 2015;**67**:266–72
23. Liu L, Akkoyunlu M. Circulating CD138 enhances disease progression by augmenting autoreactive antibody production in a mouse model of systemic lupus erythematosus. *J Biol Chem* 2021;**297**:101053
24. Cholok D, Lee E, Lisiecki J, Agarwal S, Loder S, Ranganathan K, Qureshi AT, Davis TA, Levi B. Traumatic muscle fibrosis: from pathway to prevention. *J Trauma Acute Care Surg* 2017;**82**:174–84
25. Lieber RL, Ward SR. Cellular mechanisms of tissue fibrosis. 4. Structural and functional consequences of skeletal muscle fibrosis. *Am J Physiol Cell Physiol* 2013;**305**:C241–52

(Received December 26, 2022, Accepted May 28, 2023)